IEEE Access
Multidisciplinary ⋮ Rapid Review ⋮ Open Access Journal

Received 26 October 2022, accepted 7 November 2022, date of publication 14 November 2022,
date of current version 5 December 2022.

Digital Object Identifier 10.1109/ACCESS.2022.3222359

RESEARCH ARTICLE

A Full-Wave Discontinuous Galerkin Time-Domain Finite Element Method for Electromagnetic Field Mode Analysis

HOMA ARAB[1], (Member, IEEE), DESONG WANG[2], (Student Member, IEEE), KE WU[2], (Fellow, IEEE), AND STEVEN DUFOUR[1], (Member, IEEE)
[1]Mathematic and Industrial Engineering Department, Polytechnique Montréal, Montréal, QC H3T 1J4, Canada
[2]Electrical Engineering Department, Polytechnique Montréal, Montréal, QC H3T 1J4, Canada

Corresponding author: Homa Arab (homa.arab@polymtl.ca)

This work was supported by the Fonds de Recherche du Québec–Nature et Technologies (FRQNT).

ABSTRACT The accurate analysis and the characterization of guided-wave structures are important steps in the design of microwave and optical systems. A numerical methodology based on a three-dimensional discontinuous Galerkin time-domain (DGTD) finite element method is used to estimate the resonant frequencies of various structures in a single run, with several polychromatic sources (dipole, plane wave, etc). The proposed approach leads to simulations that are fast and accurate, this being the result of the local discretization strategy of the full-wave time-domain Maxwell's equations on unstructured tetrahedral meshes that is easy to parallelize. The stability of the overall numerical scheme is obtained using an upwind numerical flux and an implicit second-order accurate time integration scheme. The numerical methodology is verified based on two problems with closed-form solutions. First, homogeneous and non-homogeneous waveguides are studied using the proposed methodology. The WR-284 waveguide is used, and cut-off frequencies of the first 7 modes are computed and compared with analytical solutions. Propagation characteristics of mode-selective transmission lines (MSTL) are then investigated. These MSTL simulation results are verified using measurement results of fabricated MSTL, microstrip, and RWG prototypes up to 110 GHz. Simulation results show the flexibility, the robustness, and the high accuracy of the proposed numerical strategy.

INDEX TERMS Rectangular waveguides, mode-selective transmission lines non-homogeneous waveguides, gradient-index materials, cut-off frequency, dispersion, electromagnetic analysis, electromagnetic fields, time-domain analysis, discontinuous Galerkin finite element method, numerical modeling.

I. INTRODUCTION

The analysis of electromagnetic fields has been the subject of numerous studies over the past decades. The main two conductor structures that can support verious TE, TM, and TEM mode wave propagations are waveguides and transmission lines. In this paper, a numerical method is proposed for analyzing waveguides and mode-selective transmission line (MSTL).

Several authors have analyzed waveguides problem in the literature. Their shape and cut-off frequency influence the design of microwave, millimeter-wave, and optic components, such as filters [1], [2], [3], [4], [5], tuners [6], [7], phase shifters [8], [9], attenuators [10], and circulator elements [11], [12]. Waveguides can be filled with a homogeneous or non-homogeneous dielectric medium. Propagation characteristics of MSTL are then investigated. MSTL is studied theoretically and experimentally by some researchers [13], [14]. This type of transmission line has frequency-dependent mode-switching behavior and is among low-loss and low-dispersion transmission line [13] The MSTL is selected to show the accuracy of the proposed numerical method to analyze the losses in materials and caused by leakage and radiation in the interface between different layers in multiplayer

The associate editor coordinating the review of this manuscript and approving it for publication was Guido Lombardi.

transmission lines. For this purpose, the time-domain full-wave Maxwell' equations are discretized on bounded 3D domains.

Maxwell's equations can give multiple solutions for a given problem. With homogeneous waveguides, two different modes exist: the transverse electric mode (TE) and the transverse magnetic mode (TM). For homogeneous rectangular or circular waveguides, the partial differential equations can be solved analytically. But for waveguides with complex shapes, or filled with non-homogeneous materials, we cannot find an analytic solution. For multilayered printed transmission line, computing the losses due to radiation and leakage are also challenging. Numerical methods, such as the finite difference method [15], [16], [17], the boundary element method [18], [19], [20], the method of moments [21], [22], [23], or the finite element method [24], [25], [26] must therefore be considered.

Various software packages, such as HFSS, ADS, CST, and FEKO, are used to perform the numerical analysis for Maxwell's equations. They are in the frequency domain (FD), or in the time domain (TD). FD methods are often more computationally costly for computing wideband frequency responses since, for each frequency, the simulation must be run completely. Some of commercial software packages are designed based on modified version of Maxwell's equations (green's functions, Helmholtz equation, H-formulation, etc.), therefore they disregarded important physics phenomena that can only be modeled using full-wave Maxwell's equations. Commercial simulation software is usually designed to study either low frequency, or high frequency problems. Using the full-wave Maxwell's equations will make the simulation software usable for various frequencies and media.

Some software packages are based on the finite-difference time-domain (FDTD) numerical method which is not very accurate for complex geometries. The finite element method (FEM) is the most popular numerical method that can be used to discretize Maxwell's equations on unstructured meshes. The FEM is a useful simulation tool for studying problems with complex geometries. But waveguides with anisotropic materials cannot be handled easily. The numerical simulation of these problems can lead to unstable approximations [27], [28]. The development of stable high-order finite element discretizations for Maxwell's equations is still an active research topic.

In order to help control numerical instabilities, some studies propose to introduce modifications to Maxwell's equations, which lead to nonphysical discrete approximations. These techniques are known for not completely succeeding in eliminating numerically induced oscillations [29], [30], [31]. Edge elements, also known as Whitney elements of degree 1, provide a cure to many problems associated with nodal-based finite element approximations [32], [33], [34]. First, they make it easier to manage discontinuous permittivities and permeabilities, since edge elements only enforce the continuity of the tangential component of the dependant variables, allowing the normal component of the vector fields to be discontinuous. They also provide more accurate approximations of vector fields near geometric singularities, such as in regions in the vicinity of sharp corners. Finally, since the numerical approximations are taken in the proper functional space, spurious modes associated with nonzero eigenvalues are reduced or eliminated. These properties come at a price, since edge elements necessitate an increased number of degrees of freedom when compared to nodal discretization techniques, which translates into simulations that necessitate more time and memory.

A fast and accurate numerical methodology based on a three-dimensional discontinuous Galerkin time-domain (DGTD) finite element method with vector basis functions (Whitney elements of degree 1) is proposed for analyzing waveguides and mode-selective transmission line (MSTL). The DGTD method does not necessitate the assembly of the contributions of the elements of the mesh in a large matrix. Instead, small local problems are discretized on each element of the mesh, which makes the method easier to parallelize [35], [36]. The numerical approximation of the discrete problem is therefore discontinuous, which adds to the flexibility provided by the Whitney element. Both homogeneous and non-homogeneous waveguides are studied to verify the proposed numerical methodology, where the cut-off frequency is computed for various modes in a single run. Propagation characteristics of MSTL are also investigated in this work. These analysis results are verified by the measured results of fabricated prototypes of MSTL, microstrip, and RWG up to 110 GHz.

II. MODELING

A. MAXWELL's EQUATIONS FOR ELECTROMAGNETIC FIELDS MODELING

The differntial form of Maxwell's equations in a limited region of interest are expressed as

$$\begin{aligned} \nabla \cdot \boldsymbol{E} &= 0 \quad \text{(Gauss's law of } \boldsymbol{E}\text{)} \\ \nabla \cdot \boldsymbol{H} &= 0 \quad \text{(Gauss's law of } \boldsymbol{H}\text{)} \\ \varepsilon \frac{\partial \boldsymbol{E}}{\partial t} - \nabla \times \boldsymbol{H} &= \boldsymbol{J} \quad \text{(Ampere's law)} \\ \mu \frac{\partial \boldsymbol{H}}{\partial t} + \nabla \times \boldsymbol{E} &= \boldsymbol{0} \quad \text{(Faraday's law)} \end{aligned} \tag{1}$$

where $\boldsymbol{H}$ is the magnetic field, $\boldsymbol{E}$ is the electric field, ε and μ represent the permittivity and permeability of the material, ρ is the charge density, and $\boldsymbol{J}$ is the current density. Dirichlet and Neumann boundary conditions must be defined as boundary conditions to have complete definition of the problem. Dirichlet condition imposed the value and Neumann condition imposed the normal derivative of the electromagnetic fields on the surface of the region.

B. INITIAL AND BOUNDARY CONDITIONS

Since the problems under study are time dependent, initial conditions $\boldsymbol{E}(\boldsymbol{x}, t_0) = \boldsymbol{E}_0(\boldsymbol{x})$ and $\boldsymbol{H}(\boldsymbol{x}, t_0) = \boldsymbol{H}_0(\boldsymbol{x})$, for all $\boldsymbol{x} \in \Omega$, allow us to compute the discrete variables $\boldsymbol{E}_h(\boldsymbol{x}, t)$ and $\boldsymbol{H}_h(\boldsymbol{x}, t)$ over the time interval $\mathbb{I} = [t_0\,, t_f]$. The appropriate

boundary values must be imposed on the surface area or perpendicular to the surface depending on the problem under study. They can be defined for the electromagnetic fields in media 1 and 2 as

$$\begin{aligned} \boldsymbol{n}\cdot(\boldsymbol{E}_1-\boldsymbol{E}_2) &= g_{\boldsymbol{E}} \quad \text{(Dirichlet)} \\ \boldsymbol{n}\times(\boldsymbol{E}_1-\boldsymbol{E}_2) &= h_{\boldsymbol{E}} \quad \text{(Neumann)} \\ \boldsymbol{n}\cdot(\boldsymbol{H}_1-\boldsymbol{H}_2) &= g_{\boldsymbol{H}} \quad \text{(Dirichlet)} \\ \boldsymbol{n}\times(\boldsymbol{H}_1-\boldsymbol{H}_2) &= h_{\boldsymbol{H}} \quad \text{(Neumann)} \end{aligned}$$

where $\boldsymbol{n}$ is the unit normal vector to Γ and $g_{\boldsymbol{E}}$, $h_{\boldsymbol{E}}$, $g_{\boldsymbol{H}}$ and $h_{\boldsymbol{H}}$ are known functions defined on $\Gamma \times \mathbb{I}$ (or with a subset of Γ). A well known example is given by the perfect electric conductor (PEC) boundary condition:

$$\begin{aligned} \boldsymbol{n}\cdot\boldsymbol{H} &= 0 \\ \boldsymbol{n}\times\boldsymbol{E} &= \boldsymbol{0} \end{aligned} \quad \text{on} \quad \Gamma\times\mathbb{I} \tag{2}$$

which can be used, as an example, with conductors at microwave frequencies. Another example is the perfect magnetic conductor (PMC) boundary condition:

$$\begin{aligned} \boldsymbol{n}\cdot\boldsymbol{E} &= 0 \\ \boldsymbol{n}\times\boldsymbol{H} &= \boldsymbol{0} \end{aligned} \quad \text{on} \quad \Gamma\times\mathbb{I} \tag{3}$$

which is often used as a symmetry boundary condition.

C. NONDIMENSIONALIZATION

Dimensionless forms are usually used to help identify the dominant physics of a given system. But from a numerical modeling point of view, it can also act as a natural preconditionner. The order of magnitude of each term of system (1) can vary significantly, which can lead to an ill-conditioned discrete problem. Given the reference quantities t_0, ℓ_0, μ_0, ε_0,, ρ_0, E_0 and H_0, we define the nondimensional variables $\tilde{t} = t/t_0$, $\tilde{\boldsymbol{x}} = \boldsymbol{x}/\ell_0$, $\tilde{\mu} = \mu/\mu_0$, $\tilde{\varepsilon} = \varepsilon/\varepsilon_0$, $\tilde{\sigma} = \sigma/\sigma_0$ $\tilde{\boldsymbol{E}} = \boldsymbol{E}/E_0$ and $\tilde{\boldsymbol{H}} = \boldsymbol{H}/H_0$. The dimensionless form of system (1), after replacing J by $\sigma\boldsymbol{E}$, then becomes:

$$\begin{aligned} \tilde{\boldsymbol{\nabla}}\cdot\tilde{\boldsymbol{E}} &= 0 \\ \tilde{\boldsymbol{\nabla}}\cdot\tilde{\boldsymbol{H}} &= 0 \\ \Pi_1\big(\tilde{\mu}\,\frac{\partial\tilde{\boldsymbol{H}}}{\partial\tilde{t}}\big) + \tilde{\boldsymbol{\nabla}}\times\tilde{\boldsymbol{E}} &= \boldsymbol{0} \\ \Pi_2\big(\tilde{\varepsilon}\,\frac{\partial\tilde{\boldsymbol{E}}}{\partial\tilde{t}}\big) - \Pi_3\,\tilde{\sigma}\,\tilde{\boldsymbol{E}} &= \tilde{\boldsymbol{\nabla}}\times\tilde{\boldsymbol{H}} \end{aligned} \tag{4}$$

where $\Pi_1 = \frac{\mu_0 H_0 \ell_0}{E_0 t_0}$, for dielectric materials $\Pi_3 \approx 0$, and $\Pi_2 = \frac{\varepsilon_0 E_0 \ell_0}{H_0 t_0}$, for conducting materials $\Pi_2 \approx 0$, and $\Pi_3 = \frac{E_0 \ell_0 \sigma_0}{H_0}$. In this study, for a unit reference magnetic field strength of $H_0 = 1\,\mathrm{A/m}$, we define the reference electric field strength as $E_0 = H_0 Z_0$ for an impedance of $Z_0 = 120\pi\ \Omega$, the reference permeability μ_0 is chosen as $4\pi \times 10^{-7}\,\mathrm{H/m}$, and the reference permittivity ε_0 is given by $8.85 \times 10^{-12}\,\mathrm{F/m}$. Finally, t_0 and ℓ_0 are problem dependent. The nondimensional quantities will be written without "$\sim$" in the remainder of the paper.

D. NUMERICAL METHODOLOGY

Industrial problems often involve complex geometries. This leads us to base this numerical study on the finite element method (FEM). Many authors discretize a modified version of system (1), which sometimes leads to ill-conditioned discrete problems. This explains why we choose to perform a direct finite element discretization of the third and fourth equations of system (1) using the discontinuous Galerkin FEM, also known as the discontinuous Galerkin time-domain (DGTD) method. In addition to the fact that it can provide a stable discrete problem, it's local nature makes it a numerical method that is easy to parallelize, which results in fast solvers for the discretization of Maxwell's equations. After discretizing the domain of definition of the problem Ω using tetrahedral elements, we obtain the finite element mesh $\Omega_h = \cup_i \mathrm{K}_i$ where element i is being denoted K_i, and where elements are not overlapping, i.e. $\mathrm{K}_i \cap \mathrm{K}_j = \varnothing$ for $i \neq j$. Let's now consider one of those tetrahedral elements K of Ω_h.

The base functional space associated with the weak forms of Maxwell's equations is expressed as

$$H(\mathrm{curl}\,;\Omega) = \left\{\boldsymbol{u} \in [L^2(\Omega)]^3 : \boldsymbol{\nabla}\times\boldsymbol{u} \in [L^2(\Omega)]^3\right\}$$

which is a variation of the $H^1(\Omega)$ Sobolev space used with classical finite element formulations, where $L^2(\Omega)$ is the set of square-integrable functions. The discrete finite element approximations $\boldsymbol{E}_h \approx \boldsymbol{E}$ and $\boldsymbol{H}_h \approx \boldsymbol{H}$ will belong to a discrete functional subspace $U_h \subset H(\mathrm{curl}\,;\Omega)$. Discrete test functions $\boldsymbol{v}_h$ and $\boldsymbol{w}_h$ will also be taken in U_h.

The classical approach consists in using the piecewise N-th order polynomial Lagrange approximation of the form

$$\begin{aligned} \boldsymbol{E}_h &= \sum_{j=1}^{4} E_j\,\boldsymbol{v}_j \\ \boldsymbol{H}_h &= \sum_{j=1}^{4} H_j\,\boldsymbol{w}_j \end{aligned} \tag{5}$$

where the E_j and H_j are scalar degrees of freedom in each node which are four for linear and ten for quadratic polynomial function. The nodal elements have the disadvantage that imposes continuous functions of the spatial variable, and they also cause difficulties near sharp corners. To overocome these problems the vectorial approximations or vectorial degrees of freedom $\boldsymbol{E}_j$ and $\boldsymbol{H}_j$ are used instead of nodal degree of freedoms. Linear edge element, also called Whitney element, is applied which is the most popular and simlest basis function were proposed by Nédélec [40].

To obtain the weak form of Faraday's law and Ampere's law, the test functions $\boldsymbol{v}$ and $\boldsymbol{w}$ must be multiplies in the equations of system (4) taken in an appropriate functional space, and we integrate over each element. The details about the process of obtainng the weak form of Maxwell's equation can be found in [41]. The weak form associated with the third and fourth equations of system (1) are

$$\int_{\mathrm{K}} \partial_t(\mu\boldsymbol{H})\cdot\boldsymbol{v}\,d\boldsymbol{x} + \int_{\mathrm{K}} (\boldsymbol{\nabla}\times\boldsymbol{E})\cdot\boldsymbol{v}\,d\boldsymbol{x}$$

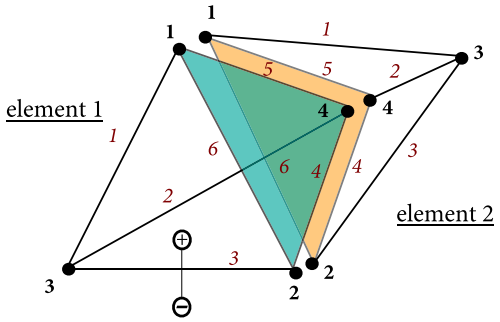

FIGURE 1. Numerical flux.

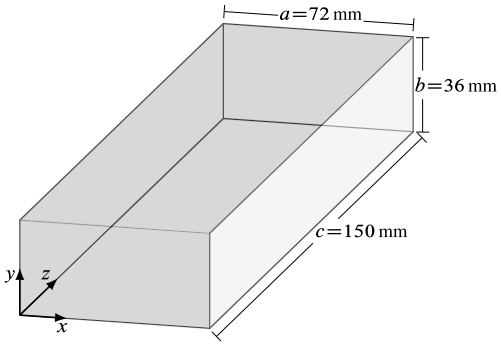

FIGURE 2. Waveguide geometry and dimensions.

$$\approx \int_{\partial \mathrm{K}} [\boldsymbol{n}\times(\boldsymbol{E}-\boldsymbol{E}^*)]\cdot \boldsymbol{v}\, d\boldsymbol{s}$$
$$\int_{\mathrm{K}} \partial_t(\varepsilon \boldsymbol{E})\cdot \boldsymbol{w}\, d\boldsymbol{x} - \int_{\mathrm{K}} (\boldsymbol{\nabla}\times \boldsymbol{H})\cdot \boldsymbol{w}\, d\boldsymbol{x} \approx$$
$$-\int_{\partial \mathrm{K}} [\boldsymbol{n}\times(\boldsymbol{H}-\boldsymbol{H}^*)]\cdot \boldsymbol{w}\, d\boldsymbol{s} \tag{6}$$

where ∂K is the boundary of element K. The right-hand side of the equations in system (6) are named flux, which is there to complete the scheme and guarantee the continuity between the solution on each edge of two neighbor elements. There are several possible choice of this flux function here we choose the up-winding flux with $Z^{\pm} = (Y^{\pm})^{-1} = \mu^{\pm}/\varepsilon^{\pm}$. The $\boldsymbol{H}^*$, and $\boldsymbol{E}^*$ are expressed in the form

$$\boldsymbol{H}^* = \frac{1}{\{\{\boldsymbol{Z}\}\}}\left(\{\{\boldsymbol{ZH}\}\} + \frac{1}{2}[\boldsymbol{E}]\right)$$
$$\boldsymbol{E}^* = \frac{1}{\{\{\boldsymbol{Y}\}\}}\left(\{\{\boldsymbol{YE}\}\} + \frac{1}{2}[\boldsymbol{H}]\right)$$

where $\{\{\boldsymbol{u}\}\}$ represents the average and $[\boldsymbol{u}]$ is used for defining the jumps along a normal vector between two elements. These notations are defined as

$$\{\{\boldsymbol{u}\}\} = \frac{\boldsymbol{u}^- + \boldsymbol{u}^+}{2}$$
$$[\boldsymbol{u}] = \hat{\boldsymbol{n}}^-\cdot \boldsymbol{u}^- + \hat{\boldsymbol{n}}^+\cdot \boldsymbol{u}^+$$

here "+" and "−" refers to the left and right side of the interface which is shown in Fig. 1. The right-hand side of the equations in system (6) can be written as

$$\boldsymbol{G_H} = \boldsymbol{n}\times\left(\boldsymbol{H}-\boldsymbol{H}^*\right) = \boldsymbol{n}\times\frac{1}{2\{\{\boldsymbol{Z}\}\}}\left(\{\{\boldsymbol{Z}^+\boldsymbol{H}\}\}-[\boldsymbol{E}]\right)$$
$$\boldsymbol{G_E} = \boldsymbol{n}\times\left(\boldsymbol{E}-\boldsymbol{E}^*\right) = \boldsymbol{n}\times\frac{1}{2\{\{\boldsymbol{Y}\}\}}\left(\{\{\boldsymbol{Y}^+\boldsymbol{E}\}\}-[\boldsymbol{H}]\right) \tag{7}$$

The M, S, and F matrices can be defined as

$$\mathbf{M} = \int_{\mathrm{K}} \boldsymbol{v}\cdot \boldsymbol{w}\, d\boldsymbol{x}$$
$$\mathbf{S} = \int_{\mathrm{K}} \boldsymbol{v}\cdot \nabla\times \boldsymbol{w}\, d\boldsymbol{x}$$
$$\mathbf{F} = \int_{\partial \mathrm{K}} \boldsymbol{v}\cdot \boldsymbol{w}\, d\boldsymbol{x} \tag{8}$$

where all these matrices are local and based on integrals of the basis functions.

$$\mathrm{M}\ \partial_t(\mu \boldsymbol{H}) + \mathrm{S}\ (\boldsymbol{\nabla}\times \boldsymbol{E}) \approx \mathrm{F}\ \boldsymbol{G_E}$$
$$\mathrm{M}\ \partial_t(\varepsilon \boldsymbol{E}) - \mathrm{S}\ (\boldsymbol{\nabla}\times \boldsymbol{H}) \approx -\mathrm{F}\ \boldsymbol{G_H} \tag{9}$$

The second-order accurate backward differentiation formula (BDF) is used to discretize the transient derivative of Maxwell's equations. The general formula for a second order BDF can be written as

$$\frac{dy(t_n+\Delta t)}{dt} \approx \frac{y(t_n+\Delta t) - \frac{4}{3}y(t_n-\Delta t) + \frac{1}{3}y(t_n-2\Delta t)}{\Delta t} \tag{10}$$

where Δt denotes the step size. The BDF is a populare implicit methods based on Lagrange interpolation polynomial for the numerical integration of ordinary differential equations, see [37]. More details of the DG-based strategy can be found in [38] and [39].

III. NUMERICAL AND EXPERIMENTAL RESULTS

The proposed numerical methodology is assessed based on a two-part analysis. The developed DGTD solver is first used to study rectangular homogeneous and non-homogeneous waveguides with known cut-off frequencies, at two different TE and TM modes. The computed numerical results are compared with closed-form analytical solutions. This approach is then used to study the behavior of MSTLs, which meets the stringent requirements for high-quality guided-wave signal propagation. The proposed MSTL is implemented and characterized for an experimental verification.

A. WAVEGUIDE

The rectangular waveguide illustrated in Fig. 2 is first studied. It is assumed that it is homogeneous with perfectly electric conducting (PEC) walls (cf. eqn (2)). A basic sinusoidal plane wave is often used as a source. Although plane wave source can be practical in some situations, it is not worth running a complete time-domain simulation to only get a system response for a single frequency. Frequency-domain methods are usually better suited in these situations. In order to obtain a wider frequency spectrum with good control over

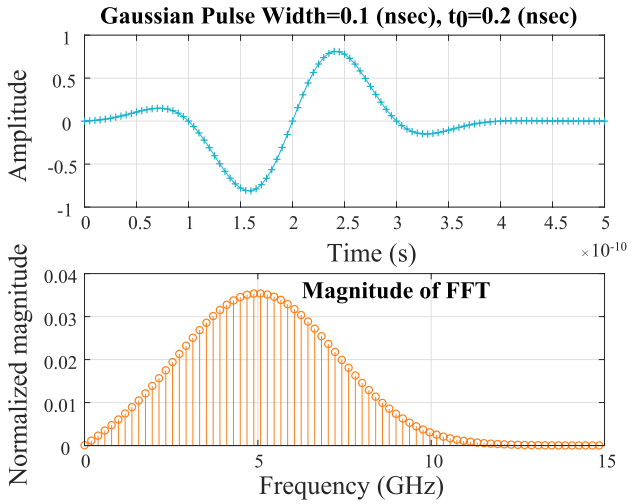

FIGURE 3. Wideband Gaussian function representation in the time domain and in the frequency domain.

the Gaussian function, modulation using a sinusoidal function is considered,

$$H_z(\boldsymbol{x}, t) = H_0 \sin(\omega t) \exp(-(t - t_0)^2/2\sigma^2)$$

where the duration σ, centered at t_0, is chosen with a frequency range of 0–10 GHz, $\omega = \pi(f_{\max} + f_{\min}) = 10\pi \times 10^9$, and $t_0 = 2 \times \sigma = 0.2 \times 10^{-9}$. The boundary conditions at the input (for $z = 0$ mm) and the output (for $z = 150$ mm) of the waveguide are therefore given by

$$\boldsymbol{H}(\boldsymbol{x}, t) = \big(0, 0, H_z(\boldsymbol{x}, t)\big)$$

Fourier transforms of the time response is used to compute the frequency response of rectangular waveguides. The Gaussian function and its Fourier transforms are illustrated in Fig. 3. A Gauss pulse is applied at a corner of the geometry, and the components of the electrical and magnetic fields are computed at the center of the waveguide. Numerical and analytical time and frequency responses of the TE mode for three components of the electromagnetic field (H_z, E_x, and E_y) are given and illustrated in Fig. 4. Numerical and analytical values of the TM mode for three components of the electromagnetic field (E_z, H_x and H_y) are given and illustrated in Fig. 5. Each peak shown in the 0–10 GHz range of the frequency response represents the mode cutoff frequency. All quantities of Figs 4 and 5 are normalized. The computed results agree with analytical solutions. As expected, the mesh grid size and the time-step size influence the accuracy of the computed approximations. In our case, the mesh grid size used is $h = 2$ mm, for a total of 0 tetrahedra, and the time-step size is $\Delta t = 5$ ps, which result in a relative nodal error of less than 1%.

The second verification problem consists of a rectangular waveguide with dimensions $8 \times 4 \times 32$ cm, which is excited for the lowest mode TE10 at a frequency of $f = 3$ GHz. In this case, the TE10 electromagnetic field is such that

$$H_z(\boldsymbol{x}, t) = \cos\left(\frac{\pi x}{8}\right) \cos(2\pi f t)$$

Two cases are considered. The first waveguide is filled with air ($\varepsilon_r = 1$ and $\mu_r = 1$). The relative permittivity of the second waveguide varies linearly from 1 to 5 over the length of the waveguide, i.e. $\varepsilon_r(\boldsymbol{x}) = \frac{1}{8}z + 1$. The computational domain Ω_h is discretized into 40, 000 tetrahedral elements, and the time-step size used is $\Delta t = 10^{-3}$. The reference quantities for the normalization are: $H_0 = 1$, $E_0 = 120\pi$, $\ell_0 = 0.1$, $f_0 = t_0^{-1} = 3$ GHz, and $\Pi_1 = \Pi_2 = 1$. Fig. 6 shows the three different components of electromagnetic field (H_x, H_z, E_y) for air field waveguides and non-homogeneous waveguides. The phase constant can be calculated from the magnitude of H_x components.

All the values in figures are normalized amount. As a source, the basic sinusoidal plane wave is chosen. Dielectric filled metallic waveguide has the same property as the air-filled one with the only exception that the cut-off frequency for the TE modes is varies in different part of waveguide due to change od dielectric properties.

The phase constant calculations are done in nine different slices where the magnetic field has their maximum values which are presented in Fig. 7a. The electromagnetic field component (H_x and E_y) along z-axis are shown in Figs. 7a, 7b. The results in Fig. 7 are in good agreement with the analytical solutions for TE10 mode for different values of relative dielectric permittivities.

B. MSTL

In this section, the numerical results of MSTL are shown to experimentally verify the capability of the proposed DGTD methods. To show the accuracy of the method, the cross-sectional electromagnetic (EM) fields in MSTL are examined, and its propagation constant is calculated and then compared with the measured and HFSS simulated results. Fig. 8 shows the structure of the proposed MSTL. The geometry dimensions and dielectric substrate properties are presented in Table 1. It consists of a homogeneous dielectric substrate of thickness h and width d with ε_r. The top and bottom planes are metals with the thickness of t and two parallel slots of size s on the top. The metal strip at the center of MSTL has the width of w. The dimensions are chosen in such a way that MSTL supports a dominant quasi-TEM mode of microstrip at lower frequency range covering DC. At the cut-off frequency, a mode conversion from the propagating quasi-TEM mode to a quasi-TE10 mode takes place. In fact, it behaves similarly to the microstrip line cases over the low frequency region and the same way as a rectangular waveguide over the higher frequency region. For experimental verification, a standard printed circuit board (PCB) process technology was adopted to implement the MSTL. The MSTL prototype is fabricated on RT/duroid 6010LM laminate from Rogers Corporation. Measurements are carried out from 10 MHz-to-110 GHz using a vector network analyzer.

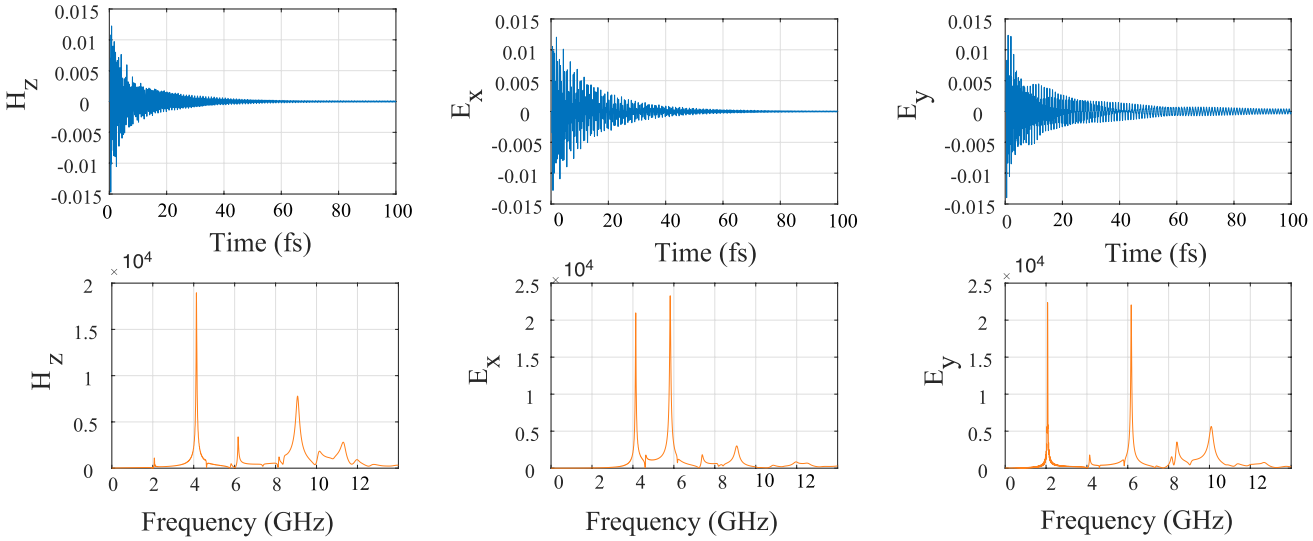

	TE10	TE20/TE01	TE11	TE21	TE30	TE31	TE40/TE02
simulation	2.078	4.158	4.649	5.889	6.248	7.493	8.330 4.157
analytical	2.082	4.167	4.658	5.892	6.250	7.500	8.333

FIGURE 4. Time and frequency responses of homogeneous waveguide for TE mode.

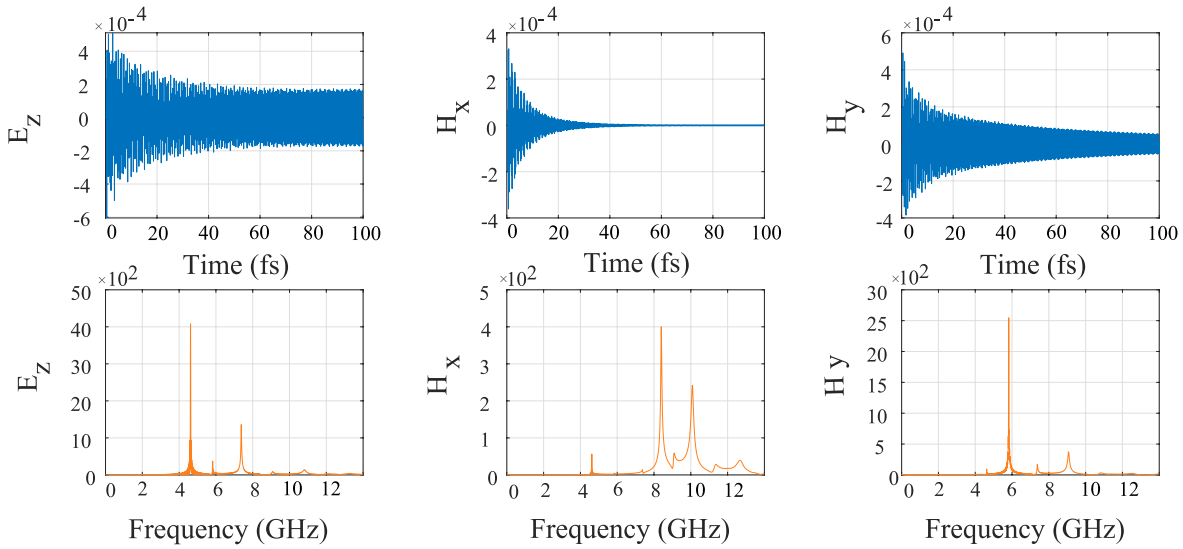

	TM11	TM21	TM31	TM41
simulation	4.636	5.878	7.424	9.288
analytical	4.658	5.892	7.500	9.300

FIGURE 5. Time and frequency responses of homogeneous waveguide for TM mode.

More details about the fabricated MSTL can be find in [14] and [42]

For numerical verification, the solution domain is discretized into 229, 282 tetrahedral elements. The problem geometry is decomposed into eight subdomains and Message Passing Interface (MPI) and domain decomposition techniques are applied to make the simulation distribute on various processors of a parallel computer [43]. The Whitney basis function or edge elements are used as basis functions because of stability and consistency properties specially for eliminating spurious solutions at the interface of two layers in MSTL systems. In oreder to have a good compromise between accuracy and computational cost the time step of 0.5×10^{-3} is chosen.

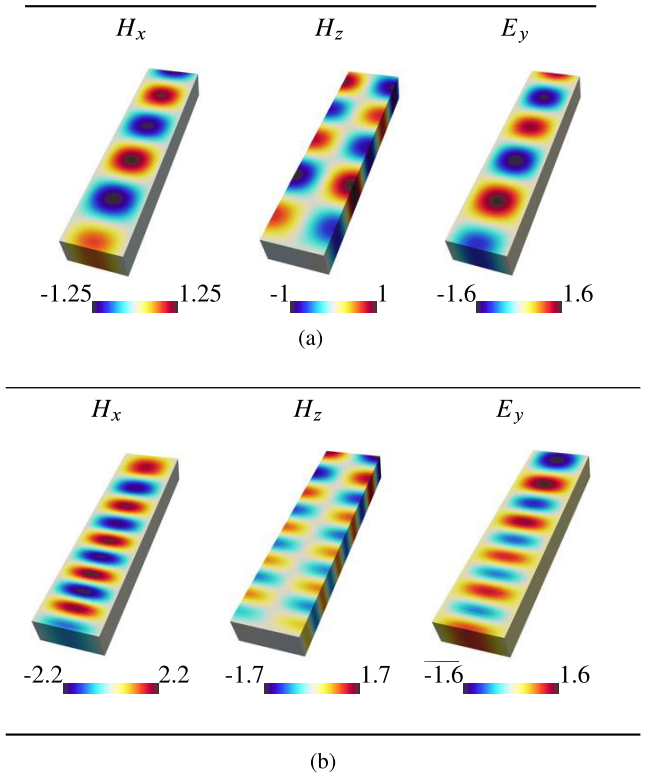

FIGURE 6. Electric and magnetic field distribution for TE10 mode in (a) air field waveguide (b) non-homogenious waveguide.

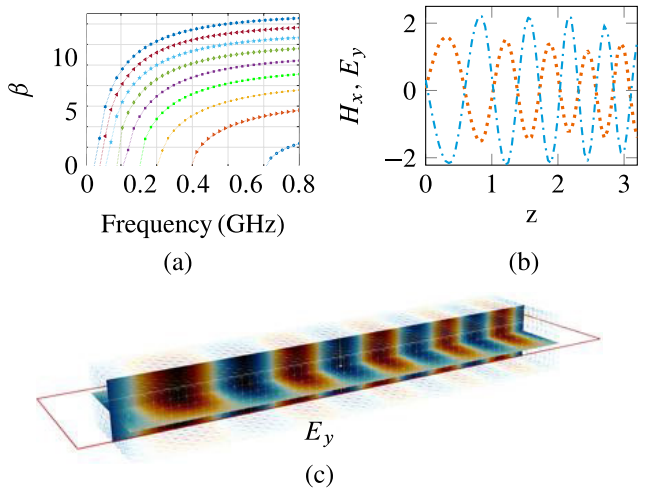

FIGURE 7. a) Dispersion curves at different surfaces of the waveguide for different values of ε_r. b) H_x, and E_y along z-axis. c) The y component of the electric field inside the non-homogeneous waveguide.

The different components of the magnetic field (H_x, H_y, H_z) and electric field (E_x, E_y, E_z) at two different frequencies of 100 GHz, and 10 GHz along x-axis are depicted in Figs. 10, and 11. As expected, all the components of electric and magnetic fields have a noticeable change in their distribution shape and magnitude in various time steps specially around slots. A sketch of the electric and magnetic field lines for the dominant quasi-TE10 waveguide mode of

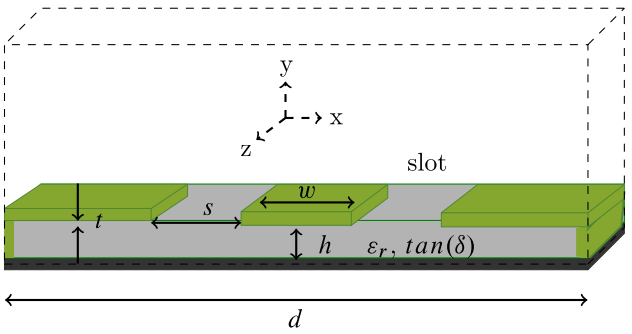

FIGURE 8. Cross section view of MSTL.

TABLE 1. Geometrical and dielectric substrate parameters.

h	d (mm)	w (mm)	s (mm)	t (μm)
0.254	3	0.65	0.25	18

ε_r	tan(δ)	σ
10.2	0.0023	5.8×10^7

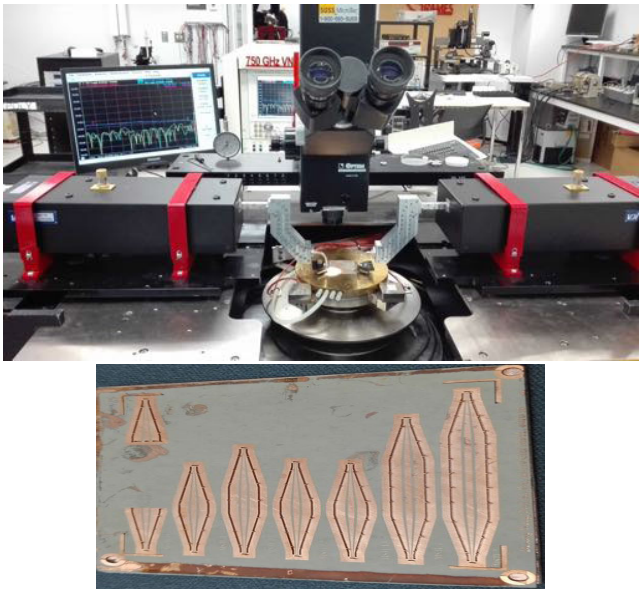

FIGURE 9. Measurements set-up and fabricated prototype.

MSTL at 100 GHz are shown in Fig. 12. It can be observed that MSTL should have the guided wave performance similar to that of a dielectric-filled RWG when frequency is higher than cut of frequency.

Phase and attenuation constant curves calculated using different method are plotted in Figs. 13a, 13b. As it shows, excellent agreement between numerical, HFSS, and experimental results is observed. It is confirmed that the low–dispersion and low–loss behavior of MSTL makes it an outstanding integrated waveguide in support of high-performance super-broadband signal transmission and/or ultra-fast pulse propagation in a fully-integrated platform. In order to evaluate

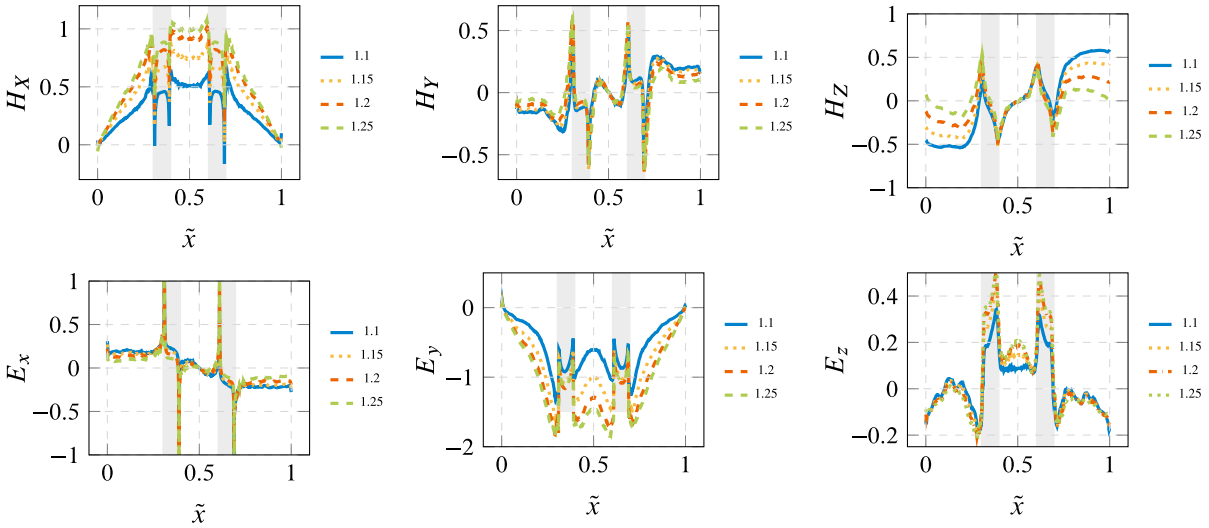

FIGURE 10. Normalized electromagnetic field distributions of MSTL along x-axis at various times and f = 100 GHz.

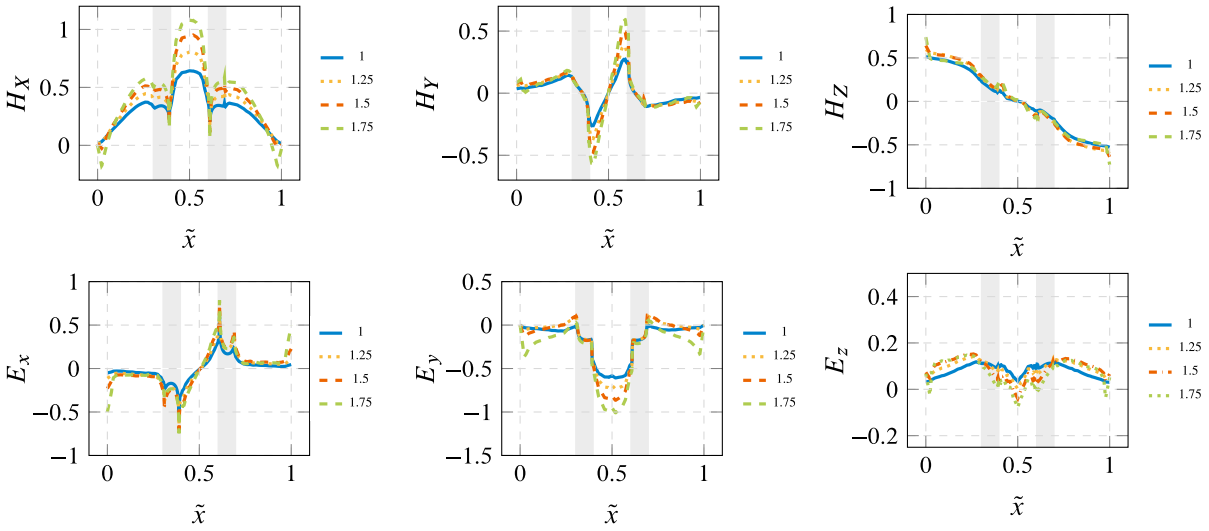

FIGURE 11. Normalized electromagnetic field distributions of MSTL along x-axis at various times and f = 10 GHz.

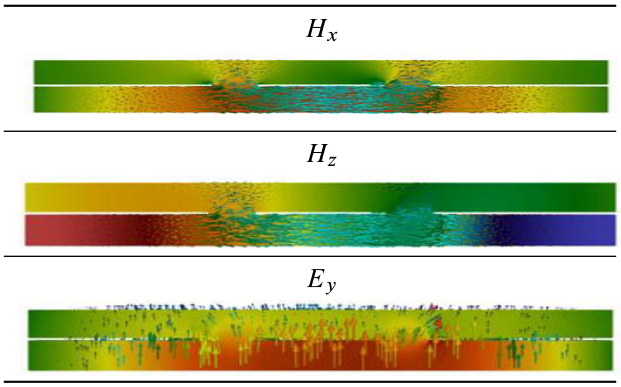

FIGURE 12. Electromagnetic field distribution in the cross section of MSTL at 100 GHz. The arrows of the electric and magnetic fields are sketched.

the effect of the basis functions, linear and quadratic nodal polynomial orders (P_1, P_2), and Whitney basis functions are implied in the developed code. The computational requirements of the simulator for one period of time are demonstrated in TABLE 2. The Euclidean norm of the error between experimental and numerical results for phase constant at $\tilde{t} = 0.125$ are plotted in Fig. 13c. This error is measured for linear and quadratic Lagrange type nodal elements and Whitney edge elements. The error values are depicted as a function of maximum edge length (h). The results show that the

TABLE 2. Degree of freedoms (DoFs), CPU time and the memory requirements for various basis functions.

	#DoF	%Time	%RAM	Δt
DGTD-P_1	23,052	63.07	34	0.5×10^{-3}
DGTD-P_2	57,630	100.00	84	0.5×10^{-3}
DGTD-Whitney	69,156	76.92	100	0.5×10^{-3}

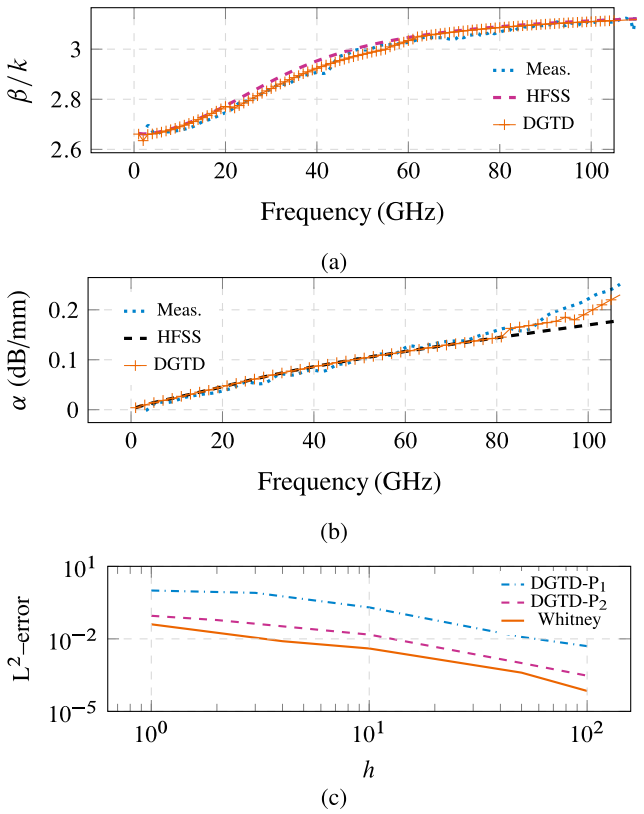

FIGURE 13. a) Comparison between DGTD, HFSS, and measurement results for normalized phase constants of the proposed MSTL. b) Comparison between DGTD, HFSS, and measurement results for Attenuation constant (α) of the proposed MSTL. c) The discrete L^2-error for phase constant obtained using DGTD with central fluxes, for different degrees of basis functions.

dispersion error reduce notably by decreasing the mesh size (h) for second order nodal and Whitney basis functions. However, using Whitney edge element requires a large number of DoFs which resulting increase in computation cost (memory and time). To compensate this issue, the geometry is divided in not very fine mesh and Whitney basis function is applied. The presented method has no limitation for applications, and the processing time is all depend to the processor we used. For presented problem, we use 4 GHz Intel Core i7, memory: 32 GB 1867 MHz DDR3. For more complicated problem we need more power full processor and more memorry.

This paper, for the first time, analyze the full-wave time-domain Maxwell's equations in a 3D structure for modeling electromagnetic field propagation in three layers MSTL system. The electromagnetic field components at the interface between layers are computed accurately. Several authors have studied the DGTD method for Maxwell's equations, and their results prove that the DGTD exhibits better consistency, stability and convergence properties when compared to the standard FEM. These advantages are because of the element-based computation nature of DGTD and having a local elements strategy [44], [45]. In this section, it is proven that the acceptable results can be obtained (in comparison to measurement results) with a relatively larger time step and mesh size ($h = 0.01$, and $\Delta t = 0.5 \times 10^{-3}$) which demonstrate the high stability of DGTD in compared to FEM. Using MPI parallel computer library reduces the numerical computational time significantly.

IV. CONCLUSION

In this paper, a 3D time domain DGTD has been introduced to analyze the electromagnetic field propagation problem. As a first example, the electromagnetic field inside homogeneous and non-homogeneous waveguides are approximated and the resonant frequencies are estimated. The developed code has capability to give us all required information in a single run for different polychromatic sources. The accuracy and efficiency of present algorithms are assessed in comparison with the analytical and measurement results. In the second verification problem, the developed simulator is used for the first time to study the behavior of MSTL. The phase constants and attenuation are measured for specific MSTL geometry and compared with measurement and HFSS software results. The DGTD method can analyze accurately the losses in matrials and caused by leakage and radiation in the interface between different layers in multiplayer transmission lines. The DGTD is an implicit variant of FEM that equations are discretized using an element-by-element strateg. This property of DGTD leads to better convergence rates and lower computational cost specially for complex multilayered geometries. In addition, the proposed method can be used in various frequency ranges, complex geometries, non-homogeneous materials, different excitation modes, etc. MPI paralle computers technique makes the proposed implementation of the DGTD solver significantly faster. The combination of the DGTD method, Whitney basis function, and applying MPI techniques are the components of the proposed numerical methodology that makes the developed solver faster and more stable than commercial codes. The developed code was validated based on both theoretical and measurement results.

REFERENCES

[1] A. Vosoogh, A. A. Brazález, and P.-S. Kildal, "A V-band inverted microstrip gap waveguide end-coupled bandpass filter," *IEEE Microw. Wireless Compon. Lett.*, vol. 26, no. 4, pp. 261–263, Apr. 2016.

[2] Y. D. Dong, T. Yang, and T. Itoh, "Substrate integrated waveguide loaded by complementary split-ring resonators and its applications to miniaturized waveguide filters," *IEEE Trans. Microw. Theory Techn.*, vol. 57, no. 9, pp. 2211–2223, Sep. 2009.

[3] J. R. Sánchez, C. Bachiller, M. Juliá, V. Nova, H. Esteban, and V. E. Boria, "Microwave filter based on substrate integrated waveguide with alternating dielectric line sections," *IEEE Microw. Wireless Compon. Lett.*, vol. 28, no. 11, pp. 990–992, Nov. 2018.

[4] Z. He, C. J. You, S. Leng, X. Li, and Y.-M. Huang, "Compact bandpass filter with high selectivity using quarter-mode substrate integrated waveguide and coplanar waveguide," *IEEE Microw. Wireless Compon. Lett.*, vol. 27, no. 9, pp. 809–811, Sep. 2017.

[5] R. Dahle, P. Laforge, and J. Kuhling, "3-D printed customizable inserts for waveguide filter design at X-Band," *IEEE Microw. Wireless Compon. Lett.*, vol. 27, no. 12, pp. 1080–1082, Dec. 2017.

[6] A. Semnani, M. A. Khater, Y.-C. Wu, and D. Peroulis, "An electronically tunable high-power impedance tuner with integrated closed-loop control," *IEEE Microw. Wireless Compon. Lett.*, vol. 27, no. 8, pp. 754–756, Aug. 2017.

[7] W. Bai, Q. Wang, X. Tian, and H. Zhang, "A quasi-planar waveguide tuner," *IEEE Microw. Wireless Compon. Lett.*, vol. 26, no. 4, pp. 228–230, Apr. 2016.
[8] J. Dittloff, F. Arndt, and D. Grauerholz, "Optimum design of waveguide E-plane stub-loaded phase shifters," *IEEE Trans. Microw. Theory Techn.*, vol. MTT-36, no. 3, pp. 582–587, Mar. 1988.
[9] E. Villa, B. Aja, J. Cagigas, E. Artal, and L. de la Fuente, "Four-state full Q-band phase shifter using smooth-ridged waveguides," *IEEE Microw. Wireless Compon. Lett.*, vol. 27, no. 11, pp. 995–997, Nov. 2017.
[10] D.-S. Eom and H.-Y. Lee, "Broadband half mode substrate integrated waveguide attenuator in 7.29–14.90 GHz," *IEEE Microw. Wireless Compon. Lett.*, vol. 25, no. 9, pp. 564–566, Sep. 2015.
[11] W. D'Orazio and K. Wu, "Substrate-integrated-waveguide circulators suitable for millimeter-wave integration," *IEEE Trans. Microw. Theory Techn.*, vol. 54, no. 10, pp. 3675–3680, Oct. 2006.
[12] K. Oshiro, H. Mikami, S. Fujii, Terumitsu Tanaka, H. Fujimori, M. Matsuura, and S. Yamamoto, "Fabrication of circulator with coplanar wave guide structure," *IEEE Trans. Magn.*, vol. 41, no. 10, pp. 3550–3552, Oct. 2005.
[13] F. Fesharaki, T. Djerafi, M. Chaker, and K. Wu, "Guided-wave properties of mode-selective transmission line," *IEEE Access*, vol. 6, pp. 5379–5392, 2018.
[14] D. Wang and K. Wu, "Mode-selective transmission line—Part I: Theoretical foundation and physical mechanism," *IEEE Trans. Compon., Packag., Manuf. Technol.*, vol. 10, no. 12, pp. 2072–2086, Nov. 2020.
[15] K. Pontoppidan, "Numerical solution of waveguide problems using finite difference methods," in *Proc. 1st Eur. Microw. Conf.*, Oct. 1969, pp. 99–102.
[16] G. Mur, "A finite difference method for the solution of electromagnetic waveguide discontinuity problems," in *Proc. 3rd Eur. Microw. Conf.*, Oct. 1973, pp. 1–4.
[17] C. ping Yu and H. chun Chang, "Modal analysis of photonic crystal planar waveguides using a finite difference method," in *Proc. Lasers Electro-Opt., CLEO/Pacific Rim, 5th Pacific Rim Conf.*, vol. 1, Dec. 2003, p. 349.
[18] M. Koshiba and M. Suzuki, "Application of the boundary-element method to waveguide discontinuities (short paper)," *IEEE Trans. Microw. Theory Techn.*, vol. MTT-34, no. 2, pp. 301–307, Feb. 1986.
[19] T. Lu and D. Yevick, "A vectorial boundary element method analysis of integrated optical waveguides," *J. Lightw. Technol.*, vol. 21, no. 8, pp. 1793–1807, Aug. 2003.
[20] D. Dobbelaere, H. Rogier, and D. D. Zutter, "Analytic properties of dispersion curves for efficient eigenmode analysis of isotropic waveguides using a boundary element method," in *Proc. Int. Conf. Numerical Electromagn. Modeling Optim. RF, Microw., THz Appl. (NEMO)*, May 2014, pp. 1–4.
[21] R. Bunger and F. Arndt, "Moment-method analysis of arbitrary 3-D metallic N-port waveguide structures," *IEEE Trans. Microw. Theory Techn.*, vol. 48, no. 4, pp. 531–537, Apr. 2000.
[22] S. G. Diamantis, A. P. Orfanidis, and G. A. Kyriacou, "Conical horn antennas employing an offset moment method and mode matching technique," *IEEE Trans. Magn.*, vol. 45, no. 3, pp. 1092–1095, Mar. 2009.
[23] A. Belenguer, H. Esteban, V. E. Boria, C. Bachiller, and J. V. Morro, "Hybrid mode matching and method of moments method for the full-wave analysis of arbitrarily shaped structures fed through canonical waveguides using only electric currents," *IEEE Trans. Microw. Theory Techn.*, vol. 58, no. 3, pp. 537–544, Mar. 2010.
[24] A. Schultschik, O. Farle, and R. Dyczij-Edlinger, "A model order reduction method for the finite-element simulation of inhomogeneous waveguides," *IEEE Trans. Magn.*, vol. 44, no. 6, pp. 1394–1397, Jun. 2008.
[25] T. Yasui, M. Koshiba, and Y. Tsuji, "A wide-angle finite element beam propagation method with perfectly matched layers for nonlinear optical waveguides," *J. Lightw. Technol.*, vol. 17, no. 10, pp. 1909–1915, Oct. 1999.
[26] T. Fujisawa and M. Koshiba, "Finite-element mode-solver for nonlinear periodic optical waveguides and its application to photonic crystal circuits," *J. Lightw. Technol.*, vol. 23, no. 1, pp. 382–387, Jan. 2005.
[27] D. Sun, J. Manges, X. Yuan, and Z. Cendes, "Spurious modes in finite-element methods," *IEEE Antennas Propag. Mag.*, vol. 37, no. 5, pp. 12–24, Oct. 1995.
[28] J. F. Lee, D. K. Sun, and Z. Cendes, "Full-wave analysis of dielectric waveguides using tangential vector finite elements," *IEEE Trans. Microw. Theory Techn.*, vol. 39, no. 8, pp. 1262–1271, Aug. 1991.
[29] A. J. Kobelansky and J. P. Webb, "Eliminating spurious modes in finite-element waveguide problems by using divergence-free fields," *Electron. Lett.*, vol. 22, no. 11, pp. 569–570, May 1986.
[30] K. Hayata, M. Koshiba, M. Eguchi, and M. Suzuki, "Vectorial finite-element method without any spurious solutions for dielectric waveguiding problems using transverse magnetic-field component," *IEEE Trans. Microw. Theory Techn.*, vol. MTT-34, no. 11, pp. 1120–1124, Nov. 1986.
[31] X. Yuan, D. R. Lynch, and K. Paulsen, "Importance of normal field continuity in inhomogeneous scattering calculations," *IEEE Trans. Microw. Theory Techn.*, vol. 39, no. 4, pp. 638–642, Apr. 1991.
[32] J.-F. Lee, G. M. Wilkins, and R. Mitra, "Finite-element analysis of axisymmetric cavity resonator using a hybrid edge element technique," *IEEE Trans. Microw. Theory Techn.*, vol. 41, no. 11, pp. 1981–1987, Nov. 1993.
[33] S.-C. Lee, J.-F. Lee, and R. Lee, "Hierarchical vector finite elements for analyzing waveguiding structures," *IEEE Trans. Microw. Theory Techn.*, vol. 51, no. 8, pp. 1897–1905, Aug. 2003.
[34] D. R. Tanner and A. F. Peterson, "Vector expansion functions for the numerical solution of Maxwell's equations," *Microw. Opt. Technol. Lett.*, vol. 2, no. 9, pp. 331–334, Sep. 1989.
[35] G. Cohen, X. Ferrieres, and S. Pernet, "Discontinuous Galerkin methods for Maxwell's equations in the time domain," *Comp. Rendus Phys.*, vol. 7, no. 5, pp. 494–500, Jun. 2006.
[36] G. Cohen, X. Ferrieres, and S. Pernet, "A spatial high-order hexahedral discontinuous Galerkin method to solve Maxwell's equations in time domain," *J. Comput. Phys.*, vol. 217, no. 2, pp. 340–363, Sep. 2006.
[37] H. Gao, "Unconditional optimal error estimates of BDF–Galerkin FEMs for nonlinear thermistor equations," *J. Sci. Comput.*, vol. 66, no. 2, pp. 504–527, Feb. 2015.
[38] J. S. Hesthaven and T. Warburton, *Nodal Discontinuous Galerkin Methods: Algorithms, Analysis, and Applications*. Springer, 2007.
[39] J. Jin, *The Finite Element Method in Electromagnetics*, 3rd ed. Hoboken, NJ, USA: Wiley, 2014.
[40] J. C. Nédélec, "Mixed finite elements in *R*," *Numer. Math.*, vol. 35, pp. 315–341, Sep. 1980.
[41] B. Arabsalmanabadi, H. Arab, V. H. G. Amador, S. Dufour, and K. Al-Haddad, "A three-dimensional discontinuous Galerkin time-domain finite element method for electromagnetic modeling of wireless power transfer coils," *IEEE Open J. Ind. Electron. Soc.*, vol. 2, pp. 360–371, 2021.
[42] D. Wang and K. Wu, "Mode-selective transmission line—Part II: Excitation scheme and experimental verification," *IEEE Trans. Compon., Packag., Manuf. Technol.*, vol. 11, no. 2, pp. 260–272, Dec. 2020.
[43] B. Barney, "Message passing interface (MPI)," Lawrence Livermore Nat. Lab., Tech. Rep., 2015.
[44] Q. Ren, J. Nagar, L. Kang, Y. Bian, P. Werner, and D. H. Werner, "Efficient wideband numerical simulations for nanostructures employing a drude-critical points (DCP) dispersive model," *Sci. Rep.*, vol. 7, no. 1, pp. 1–10, Dec. 2017.
[45] J. Alvarez, L. D. Angulo, A. R. Bretones, and S. G. Garcia, "3-D discontinuous Galerkin time-domain method for anisotropic materials," *IEEE Antennas Wireless Propag. Lett.*, vol. 11, pp. 1182–1185, 2012.

HOMA ARAB (Member, IEEE) was born in Iran. She received the master's degree in telecommunications engineering from the École Polytechnique de Montréal, and the Ph.D. degree in telecommunications from the Institut National de la Recherche Scientifique (INRS)—Centre Énergie Matériaux Télécommunications, Montréal, Canada. She worked for the Control and Protection Department, Moshanir Company, from 2005 to 2011. She is currently a Postdoctoral Fellow with the École Polytechnique de Montréal. Her current research interests include microwave and millimeter-wave circuit design, transmitter and receivers, radars, and dielectric measurements.

DESONG WANG (Student Member, IEEE) received the B.Sc. degree in electronic information engineering from Anhui University, Hefei, China, in 2010, and the M.Sc. degree in electronic engineering from the Nanjing University of Science and Technology, Nanjing, China, in 2013. He is currently pursuing the Ph.D. degree in electrical engineering with the École Polytechnique of Montréal (University of Montréal), Montréal, QC, Canada. He was a Research Assistant at the City University of Hong Kong, Hong Kong, SAR, China, from 2013 to 2016. From August 2012 to January 2013, he was an Exchange Student with Chang Gung University, Taiwan, China. His current research interests include mm-wave and THz broadband transmission lines and applications.

KE WU (Fellow, IEEE) received the B.Sc. degree (Hons.) in radio engineering from Southeast University, Nanjing, China, in 1982, and the D.E.A. and Ph.D. degrees (Hons.) in optics, optoelectronics, and microwave engineering from the Institut National Polytechnique de Grenoble, University of Grenoble, Grenoble, France, in 1984 and 1987, respectively.

He was the Director of the Poly-Grames Research Center, Montréal, QC, Canada. He was the Founding Director of the Center for Radiofrequency Electronics Research of Québec (Regroupement stratégique of FRQNT) and a Tier—I Canada Research Chair of RF and Millimeter-Wave Engineering. He has held guest, visiting, and honorary professorships with many universities. He is currently a Professor of electrical engineering and an NSERC-Huawei Industrial Research Chair of Future Wireless Technologies with the Polytechnique Montréal (University of Montreal), Montréal. He is also with the School of Information Science and Engineering, Ningbo University, Ningbo, China, on leave from his home institution, leading a special 5G and future wireless research program. He has authored or coauthored over 1100 refereed articles and a number of books/book chapters. He has filed more than 50 patents. His current research interests include substrate-integrated circuits, antenna arrays, field theory and joint field/circuit modeling, ultrafast interconnects, wireless power transmission and harvesting, megahertz-through-terahertz transceivers and sensors for wireless systems and biomedical applications, and modeling and design of microwave and terahertz photonic circuits and systems.

Dr. Wu was an Elected IEEE MTT-S Administrative Committee (AdCom) Member, from 2006 to 2015. He is currently a fellow of the Canadian Academy of Engineering and the Royal Society of Canada (The Canadian Academy of the Sciences and Humanities). He is also a member of the Electromagnetics Academy, Sigma Xi, URSI, and IEEE Eta Kappa Nu. He is the Inaugural Representative of North America as a member of the European Microwave Association General Assembly. He was a recipient of many awards and prizes including the first IEEE MTT-S Outstanding Young Engineer Award; the 2004 Fessenden Medal of the IEEE Canada; the 2009 Thomas W. Eadie Medal of the Royal Society of Canada; the Queen Elizabeth II Diamond Jubilee Medal, in 2013; the 2013 FCCP Education Foundation Award of Merit; the 2014 IEEE MTT-S Microwave Application Award; the 2014 Marie-Victorin Prize (Prix du Quebec—the Highest Distinction of Québec in the natural sciences and engineering); the 2015 Prix d'Excellence en Recherche et Innovation of Polytechnique Montréal; and the 2015 IEEE Montreal Section Gold Medal of Achievement. He has held key positions in and has served on various panels and international committees including the Chair of Technical Program Committees, International Steering Committees, and international conferences/symposia. In particular, he was the General Chair of the 2012 IEEE Microwave Theory and Techniques Society (IEEE MTT-S) International Microwave Symposium. He served on the Editorial/Review Boards of many technical journals, transactions, proceedings, and letters, as well as scientific encyclopedia, including as an editor or a guest editor. He was the Chair of the joint IEEE Chapters of MTT-S/AP-S/LEOS, Montréal. He is currently the Chair of the newly restructured IEEE MTT-S Montreal Chapter. He served as the Chair for the IEEE MTT-S Transnational Committee, the IEEE Member and Geographic Activities Committee, and the Technical Coordinating Committee among many other AdCom functions. He was an IEEE MTT-S Distinguished Microwave Lecturer, from 2009 to 2011. He was the 2016 IEEE MTT-S President.

STEVEN DUFOUR (Member, IEEE) received the B.Sc. degree in mathematics and the M.Sc. degree in applied mathematics from the Université de Montréal, and the Ph.D. degree in engineering mathematics from the École Polytechnique de Montréal. After two years as an Assistant Professor at the Department of Mathematics, University of Wyoming, USA, he returned to the Department of Mathematics and Industrial Engineering, École Polytechnique de Montréal, where he is currently an Associate Professor. He was also a Visiting Professor at Brazil (UERJ) and Saudi Arabia (KAUST). He is teaching applied mathematics to engineering students. His current research interests include the development of new finite-element based numerical methodologies for modeling fluid mechanics problems found in free surface and turbulent flows, for modeling electromagnetism phenomena found in supraconductors and for the optimization of antennas, and for the study of magnetohydrodynamics.